Applied Soft Computing Journal 93 (2020) 106383

Contents lists available at ScienceDirect

Applied Soft Computing Journal

journal homepage: www.elsevier.com/locate/asoc

Automating detection and localization of myocardial infarction using shallow and end-to-end deep neural networks

Kamal Jafarian [a,b], Vahab Vahdat [c,*], Seyedmohammad Salehi [d], Mohammadsadegh Mobin [e]

[a] Department of Electronic Systems, Aalborg University, Denmark
[b] Petricore Norway AS, Trondheim, Norway
[c] Institute for Technology Assessment, Massachusetts General Hospital, Harvard Medical School, Boston, MA, USA
[d] Department of Computer and Information Sciences, University of Delaware, Newark, DE, USA
[e] Department of Industrial and Systems Engineering, Oakland University, Rochester, MI, USA

ARTICLE INFO

Article history:
Received 26 April 2019
Received in revised form 16 January 2020
Accepted 2 May 2020
Available online 8 May 2020

Keywords:
Myocardial infarction
ECG signal processing
Deep residual learning
Artificial neural networks
Discrete wavelet transform
Principal Component Analysis

ABSTRACT

Myocardial infarction (MI), also known as a heart attack, is one of the common cardiac disorders caused by prolonged myocardial ischemia. For MI patients, specifying the exact location of a heart muscle suffering from blood shortage or stoppage is of crucial importance. Automatic localization systems can support physicians for better decisions in emergency situations. Using 12-lead electrocardiogram, in this paper, two MI detection and localization methods are proposed with classic and end-to-end deep machine learning techniques. For the feature extraction phase, the classic approach performs a Discrete Wavelet Transform (DWT) and Principal Component Analysis (PCA) on the pre-processed signals followed by a shallow neural network (NN) for the classification phase. However, in the end-to-end residual deep learning technique, a Convolutional Neural Network (CNN) is directly employed on the pre-processed input signals. For specifying the infarcted region of myocardium, 6 classes of subdiagnosis are considered. Proposed models are verified with the Physikalisch-Technische Bundesanstalt (PTB) dataset, where the data of each patient is first grouped and then carefully partitioned to training, validation, and test datasets. The results of K-fold cross-validation indicate that the general model achieves over 98% accuracy for both MI detection and localization with fewer number of feature sets compared to previous studies. Moreover, the end-to-end CNN model shows superior performance by achieving perfect results. Thus, with the larger size of CNN models, one may choose a perfect system that requires larger memory compared to another system that requires less computational power and accepts nearly 2% of false positives and/or false negatives.

1. Introduction

According to a 2016 World Health Organization (WHO) report [1], coronary heart disease, also known as ischemic heart disease, is the leading cause of death in the world. The WHO study shows over 17.7 million people die annually from cardiovascular diseases of which 80% are caused by heart attacks. Heart attacks, also called Myocardial Infarction (MI), is the result of partial or complete occlusion toward coronary arteries, leading to insufficient blood flow to the heart [2]. Interested readers are referred to Appendix for an introduction to the anatomy of coronary and MI. According to emergency guidelines [3,4], MI detection and localization must be conducted instantly on suspicious patients. The immediate assessment and therapeutic priority determination of MI not only can decrease the risk of subject's death, but also can lead to reperfusion, which prevents undergoing necrosis [3].

Patients with MI can be diagnosed by several methods including electrocardiogram (ECG) [5–9], echocardiography [10], magnetic resonance imaging (MRI) [11], and variation in cardiac biomarkers such as creatine Kinase MB (CK-MB) [12], Troponins [13], and Myoglobin [14]. In practice, the first MI diagnostic method for patients with urgent need is ECG. ECG machines are frequently available inside the ambulance and emergency rooms, providing a prompt and highly accurate diagnosis of heart failures, if being interpreted correctly [3].

Several studies have been carried out to automate MI detection by analyzing ECG signals using different machine learning and artificial intelligence methods [15–17]. The literature

* Corresponding author.
E-mail addresses: kamal.jafarian@petricore.com (K. Jafarian), vvahdatzad@mgh.harvard.edu (V. Vahdat), salehi@udel.edu (S. Salehi), mobin@oakland.edu (M. Mobin).

https://doi.org/10.1016/j.asoc.2020.106383
1568-4946/

Acronyms

ALMI	Antero-Lateral myocardial infarction
AMA	Acute Marginal Artery
AMI	Anterior myocardial infarction
ANN	Artificial Neural Networks
ASMI	Antero-Septal myocardial infarction
BW	Baseline Wander
CNN	Convolutional Neural Network
CSI	Cubic Spline Interpolation
DFT	Discrete Fourier Transform
DWT	Discrete Wavelet Transform
DNN	Deep Neural Network
EWT	Empirical Wavelet Transform
ECG	Electrocardiogram
FAWT	Flexible Analytic Wavelet Transform
ILMI	Infero-Lateral myocardial infarction
IMI	Inferior myocardial infarction
IPLMI	Infero-Postero-Lateral myocardial infarction
kNN	k-Nearest Neighbors
LA	Left Atrium
LAD	Left Anterior Descending
LCA	Left Coronary Artery
LCX	Left Circumflex
LR	Logistic Regression
LSTM	Long Short-Term Memory
LV	Left Ventricle
MI	Myocardial Infarction
ML	Machine Learning
N_{pc}	Number of Principal components
PCA	Principal Component Analysis
PCs	Principal Components
PDA	Posterior Descending Artery
PTB	Physikalisch-Technische Bundesanstalt
RA	Right Atrium
RBF	Radial axis function
RCA	Right Coronary Artery
RNN	Recurrent Neural Network
RV	Right Ventricle
STD	Standard deviation
SVM	Support Vector Machine
SWT	Stationary Wavelet Transform
VCG	Vector-cardiogram
WHO	World Health Organization
WT	Wavelet Transform

Notations

Ψ	Basis function in WT
τ	Position or time shift factor in WT
a	Scaling factor in WT
Acc	Accuracy
A_L	L^{th} Sub-band Approximation coefficient
C_{kg}	Number of samples belonging to class k but labeled as class g
D_L	L^{th} Sub-band Detail coefficients
FP	False Positive
FN	False Negative
n_k	Class k samples proportion in the data
TP	True Positive
TN	True Negative
Sn	Sensitivity
Sp	Specificity

presents several flavors of methods for ECG signal pre-processing, feature extraction, and signal classification. Sun et al. [18] employed the latent topic multiple instance learning (LTMIL) classifier to detect the presence of MI using features extracted from ST segments of each ECG signal. Chang et al. [19] examined the MI detection by Hidden Markov, Gaussian Mixture, and Support Vector Machine (SVM) classifiers on 12-lead ECG data. Waduud et al. [20] conducted an experiment on ST amplitude of 12-lead ECG and determined the culprit arteries are the left anterior descending and the right coronary artery. More recently, Dohare et al. [21] used SVM for detecting MI by determining over two hundred parameters from average beat with 10 s length in 12-lead ECG signals. However, there are still challenges in the accuracy and computational complexity of the proposed techniques.

While detecting MI is crucial, the focus of new studies is on extracting additional information from the ECG signals. For example, Adam et al. [22] used k-Nearest Neighbor (kNN) to classify ECG signals into four categories which are MI, dilated cardiomyopathy, hypertrophic cardiomyopathy, and normal. Le et al. [23] determined complex spatio-temporal patterns to detect and localize MI using vector-cardiogram (VCG) and the random-walk network along with three orthogonal planes of the body. Arif et al. [24] implemented kNN classifier and extracted time domain features of ECG beats including T wave amplitude, Q wave and ST level deviation. In order to fully detect and localize the culprit artery, a two-class and a multi-class classifier corresponding to ten regions are constructed and evaluated respectively. Acharya et al. [25] studied MI anatomical location by transforming 12-lead ECG signals to a 4-level discrete wavelet transform. From each lead, 12 nonlinear features including entropy and largest Lyapunov exponent are extracted and the optimal features are selected using a t-test feature ranking methodology. Finally, using a kNN classifier, authors evaluated their model performance under different scenarios. Sharma et al. [26] constructed different classifiers including kNN, the linear, and kernel-based SVM to first detect infarcted subjects and then localize MI pathologies into six different regions.

With the rise of deep learning methods in recent years, the majority of the research in MI detection has shifted to implementing these methods. One of the advantages of deep learning models is achieving high accuracy performance without extensive signal processing. In turn, the signals can be classified efficiently, often with fewer number of signals. For instance, Nezamabadi et al. [27] utilized a multi-scale deep convolutional neural network to extract features from chest HRCT signal. To optimize the classification performance, Wu et al. [28] developed a new deep feature learning method. The optimized features are fed into the softmax regression to build a multi-class classifier. Table 1 illustrates a survey of the most recent research studies on MI detection and localization categorized by study characteristics, signal transformations, features extraction, and classifications methods.

As discussed, many studies used traditional machine learning and deep learning techniques for detecting and localizing heart disorders such as MI, but there are major drawbacks associated with previous studies that this research seeks to address. The first shortcoming of the previous studies stems from ignoring the importance of data partitioning in the classification methods. If the data in the test dataset has been partially observed in the training dataset, model performance can be overestimated. As a

Table 1
Review of the most recent literature for detection and localization of Myocardial Infarction (**P.M.** = Proposed Method).

Features			Research studies																
			[25]	[29]	[30]	[31]	[21]	[32]	[33]	[34]	[35]	[36]	[37]	[38]	[39]	[40]	[41]	P.M. 1	P.M. 2
Study characteristics	Study type	Detection	✓	✓	✓	✓	✓	✓	✓	✓	✓	✓	✓	✓	✓	✓	✓	✓	✓
		Localization	✓					✓						✓	✓		✓	✓	✓
	Data types & preparation	Number of leads	12	1	1	3	12	12	1	1	3	3	1	8	12	12	1	12	12
		Beat analysis	✓		✓			✓	✓			✓	✓		✓		✓		
		Record analysis				✓	✓			✓	✓			✓		✓		✓	✓
		Intra-information segmentation	–	–	–	✓	✓	–	–	No	–	✓	No	No	No	✓	–	✓	✓
	Morphological analysis	ST, QRS, P wave segmentation					✓												
Transformation & decomposition methods		DWT	✓										✓		✓		✓	✓	
		FAWT			✓														
		DFT										✓							
		EWT														✓			
Feature extraction		Statistical feature investigation	✓				✓									✓			
		PCA					✓											✓	
Classification methods	Traditional ML	ANN			✓													✓	
		Random forest			✓														
		SVM			✓		✓												
		Logistic regression										✓							
		kNN	✓										✓						
	Deep learning	Deep neural network														✓			
		Decision tree															✓		
		CNN		✓		✓		✓	✓	✓	✓			✓	✓				✓
		RNN												✓					
		LSTM							✓					✓					

(–) indicates the studies that the data segmentation strategy is not well-defined or could not be justified.

result, even if the accuracy of the classifier is very high, it may fail to categorize future unseen observations reliably. Through the investigation of the current literature, only a few studies reported strategies to group the records of each patients prior to splitting data into training, test, and validation sets. Most of the studies did not segregate the data properly or did not discuss the segmentation process explicitly (shown by "–" in Table 1). The second drawback with previous studies is the lack of comprehensive modeling. Although previous studies have shown promising results, the majority of the researchers have developed models to detect the MI rather than detect and localize.

Following the drawbacks associated with previous studies, the major contributions of this research that fill the gap of the current literature are as follows:

- Previous studies overlooked the importance of proper signals partitioning for training and testing datasets. In this study, the signals of each patient are grouped to ensure that they can only be assigned to one of the partitions (i.e., train, validation, or test). Hence, the patient data will not partially be examined by the classifiers in the training phase, providing more robust performance.
- In order to build a comprehensive framework to detect and localize MI simultaneously, two classification methods are implemented and verified using the Physikalisch-Technische Bundesanstalt (PTB) database of PhysioNet bank [42]. In the first method, a classic ECG processing method with a novel configuration including hierarchical shallow neural networks (NN) are utilized in both detecting and locating MI into 6 specific infarcted regions. In the second method, an end-to-end convolutional neural network is deployed. Building both traditional and deep neural networks enable the opportunity to compare the complexity, efficiency, and accuracy of both models within one framework.
- For the traditional neural network model, several innovative techniques are used. While there is a known trade-off between the size of feature vector and the obtained accuracy from the classifier, this research builds a highly accurate model with fewer number of features extracted from ECG signals. For this purpose, a different combination of Principal Component Analysis (PCA) and Discrete Wavelet Transform (DWT) is employed to extract distinctive features from ECG signals. Using PCA, the number of signals is reduced to 7 signals from 12 (original ECG signals) in MI detection and 8 signals in MI localization phase, respectively. The results indicate that the accuracy of the classifiers reaches over 99% in detecting and 98% in locating the MI.
- By utilizing end-to-end deep neural networks, we are able to build efficient models that require only few steps to detect and localize MI from the raw signals. This advantage can harness the use of these classification method on big datasets and ease the required hardware design. Our proposed end-to-end MI detector and localizer classifier achieves perfect results for MI patients.

The rest of the paper is organized as follows. Section 2 is dedicated to our method, providing a comprehensive explanation of the proposed framework for detecting and localizing MI.

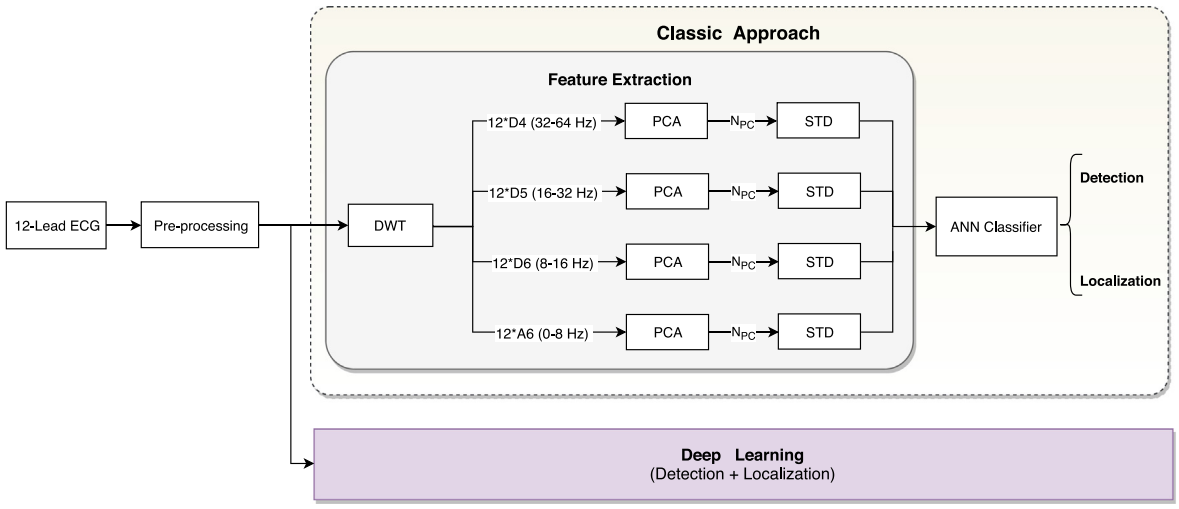

Fig. 1. A schematic diagram of steps for different approaches investigated in this study.

Section 3 presents an overview of the dataset that is used in this research. The results of the proposed models are presented in Section 4, followed by evaluation and performance discussion in Section 5. Finally, Section 6 concludes the paper with future research directions.

2. Methodology

For detection and localization of MI, two automatic methods (i.e., classic hierarchical multi-lead ECG processing system and end-to-end deep neural network) are implemented and compared. Fig. 1 represents a simplified diagram of the steps required for each of the methods. The first step, common in both methods, is signal pre-processing, while the following steps differ based on the type of technique. In classic approach, several transformations and feature extraction layers should be performed. In contrast, in end-to-end deep learning approach, the pre-processed signals are directly fed into the deep network without additional processing. In the following subsections, details pertaining to each of these methods are further explored.

2.1. Pre-processing phase

ECG signals can be corrupted by two major artifacts; first, high-frequency noise such as electromyogram (EMG) induced noise, mechanical forces on the electrodes, and power line interference, and second, baseline wander (BW) that may be caused by patient movement and respiration or destabilized instruments during the ECG recording [43,44]. Prior to analyzing the ECG signals, it is required to remove the noise from the signals while preserving signals' main informative values. In this study, as shown in Fig. 2, the residual power-line interference and its harmonics are suppressed by applying a 60-Hz notch filter with a 3-dB bandwidth of 5 Hz, also known as band-rejection filter. Moreover, a third order cubic spline interpolation (CSI) is employed to remove BW [45,46] which is capable of recovering the isoelectric level in the detrend signal. In this technique, a cubic polynomial is fitted to a set of representative points of the original ECG signal. As a result, the signal's low frequency trend can be obtained considering the reference points. The fitted baseline is then subtracted from the ECG signal to remove this artifact.

2.2. Classic hierarchical approach

After the pre-processing phase, a set of DWT and PCA transformations are performed to extract distinctive features from the signals. Utilizing the extracted features, two different shallow neural networks are trained in a hierarchical classification framework (for detection and then localization of MI), as briefly discussed in the following subsections.

2.2.1. Feature extraction

After de-noising ECG signals, signals are decomposed into the wavelet coefficients. Wavelet transform (WT) is a mathematical convolution of a signal with a specific wavelet function to represent the time–frequency characteristics of a signal. The WT of function $f(t)$ with the wavelet basis function $\Psi(\cdot)$ at scale a and position or time τ is given by:

$$W_{f(a,\tau)} = \frac{1}{\sqrt{a}} \int_{-\infty}^{+\infty} f(t)\Psi\left(\frac{t-\tau}{a}\right) dt \tag{1}$$

In order to implement the wavelets on digital signals, discrete wavelet transform (DWT) is used by a set of predefined discrete scales. To decompose signals, dyadic WT is employed that characterizes basic wavelet shape and covers the entire region of interest. Dyadic WT based on the squared dilation of the mother wavelet at the scale 2^j (or level j), is shown in Eq. (2).

$$\Psi_{2^j}(t) = \frac{1}{\sqrt{2^j}}\Psi\left(-\frac{t}{2^j}\right) \tag{2}$$

Multi-resolution decomposition of an ECG signal using dyadic WT at level L can be shown by $L+1$ sub-band coefficients including *one* approximate coefficient (A_L), and L sub-band detail coefficients, namely, $D_L, D_{L-1}, \ldots, D_1$ [47]. In this paper, a 6-level wavelet decomposition is performed for each lead of ECG signal with the *Daubechies 4* mother wavelet function. By using $L = 6$, an approximation sub-band matrix $A_6 = \left\{A_6^1, A_6^2, \ldots, A_6^m\right\}$ and six sub-band detail matrices $D_i = \left\{D_i^1, D_i^2, \ldots, D_i^m\right\}$ are constructed, where $m = 12$ is the leads number and $i = 1, 2, \ldots, 6$ is the level of coefficients [26]. A distinctive set of features can be extracted from the constructed matrices $\{A_6, D_i;\ i = 1, 2, \ldots, 6\}$.

Different statistical and spectral feature sets are experimented for this study (e.g., Standard deviation, signal power, and dominant frequency). Our analysis shows that the only feature set that has significant impact on the results is standard deviation (STD) of transformed signals. Other feature sets are eventually

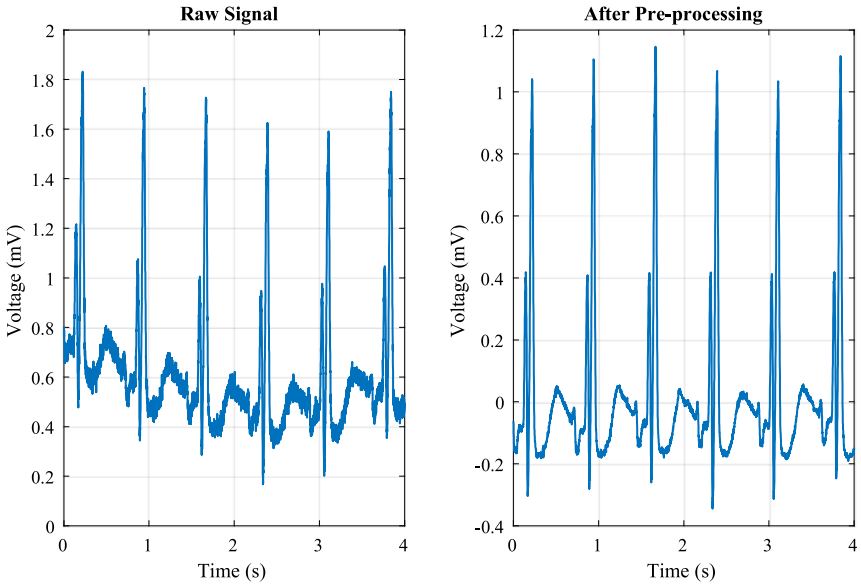

Fig. 2. Signal pre-processing including baseline wandering and power line artifact rejection.

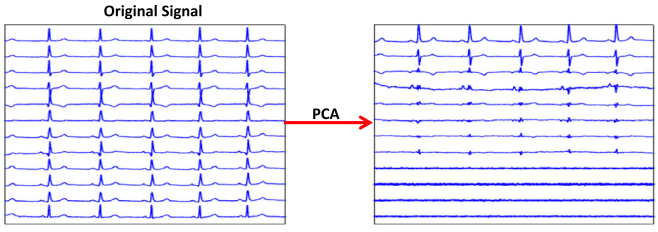

Fig. 3. Applying PCA on original ECG signal. While PCA can reduce the dimensions of study, it can inversely affect full extraction of information from the signal.

removed from the analysis while the entire set of final features is still statistically significant with p-value of less than 0.01.

In our study, most of the region of interest lies in the lower frequency sub-band coefficients, as also inspected by previous studies [48]. As a result, we only take $\{A_6, D_6, D_5, D_4\}$ for further feature extraction. The first three level detail coefficients $\{D_3, D_2, D_1\}$ hold relatively high-frequency contents (larger than 62.5 Hz) in comparison with the natural heart activities. This also demonstrates that implementation of a high-frequency noise rejection filter was unnecessary in the pre-processing step.

2.2.2. Principal component analysis

After decomposing the signals, PCA is used to extract the temporal deviations of ECG signals. PCA serves as a dimension reduction method to represent underlying variations of the data in a fewer linearly independent features [49]. Using PCA, the constructed matrices including A_6, D_6, D_5 and D_4 are projected into a new mutually uncorrelated space [50]. As the number of selected principal components (N_{pc}) increases, the variation of signal decreases, albeit cumulative variation covered by the model increases. Several frequency and time-domain features can be extracted from the developed signals. For this purpose, standard deviation of each derived signal is computed to quantify the amplitude dispersion from the mean value. Different values for N_{pc} are tested for feature extraction, and the classifier's performance is assessed. Thus, each matrix in $\{A_6, D_6, D_5, D_4\}$ produces k standard deviations, and entirely $4 \times k$ features are extracted for classification.

While combining PCA and DWT has been used by other researchers, we revised the sequence of combining these methods to achieve better results. Previously, PCA has been widely used in pre-processing phase for dimension reduction purpose and then followed by DWT on the reduced number of signals. However, using PCA in pre-processing phase, as shown in Fig. 3, could impair the extraction of main information in the signal. This is as a result of the fact that the 12-lead ECG signals have disparate frequency resolutions. Thus, the lower frequency lead ECGs are always suppressed by PCA, even if carrying useful information. In this research, PCA is performed on the distinctive set of features that is extracted from DWT, or specifically $\{A_6, D_6, D_5, D_4\}$. Each set of these features have similar frequency resolutions and applying PCA will find maximum variation correspond to that frequency resolution, preserving information from different range of signal frequencies. As shown in Fig. 4, applying PCA on the extracted feature will not disregard the important information on each signal, and therefore, will improve the accuracy of the classification model.

2.2.3. Classification using shallow neural network

In the first approach, shallow neural networks (NN) classifiers are used to detect and localize MI in a hierachical classification mode. NN is a network of neurons that receive series of inputs and use a propagation function to produce outputs based on their internal states. Outputs of neurons will be served as inputs of next-layer neurons forming a directed, weighted graph. The properties of the trained NN is as follows. A three-layer neural network is constructed by $4 \times N_{pc}$ input nodes from the extracted features. The number of hidden layers are the summation of output layer and $\frac{2}{3}$ of the input layer size, as recommended by [51]. The output layer consists of two nodes for detection of infarcted patients from healthy individuals, and six nodes for localization of MI cases. Layers in the network are fully connected. In addition, the network is trained such that each input vector results in an output vector with a non-zero element corresponding to the predicted class label. The NN classifiers are trained by Levenberg–Marquardt back-propagation algorithm [52,53]. Unlike other back-propagation algorithms, Levenberg–Marquardt algorithm calculates the approximation of loss, the gradient, and the Hessian matrices rather than computing the exact values. Then, in order to minimize the loss at each iteration, the damping

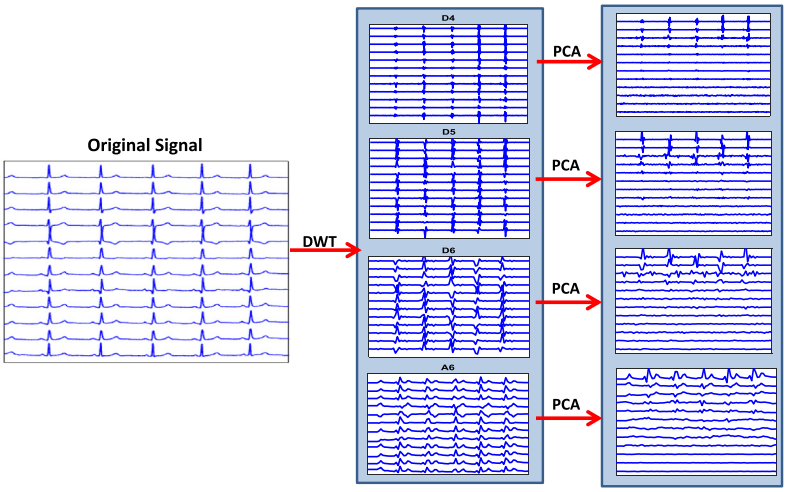

Fig. 4. Implementation of PCA method in this research. Instead of using PCA on the original ECG signals, it is used on distinctive set of features that are extracted from DWT.

parameter is adjusted. The learning procedure is continued either until 30 validation failures are observed or when the maximum number of iterations (i.e., 100 epochs) is reached.

2.3. End-to-end deep residual learning with dilated convolutions

Deep residual learning, originally conceived for image recognition applications, was proposed by He et al. [54] in order to overcome the performance degradation that occurs in convolutional neural networks (CNNs) when the number of hidden layers is large. In short, the idea behind deep residual learning is as follows. Let l designate a particular layer of a neural network such that $\mathbf{x}_{l-1}$ represents its input. The authors of [54] stated that when networks are too deep, instead of optimizing the original mapping $\mathcal{F}_l^{l+k}(\mathbf{x}_{l-1})$ between layers l and $l+k$ ($k \in \mathbb{N}$), it might be easier to optimize the residual mapping $\mathcal{H}_l^{l+k}(\mathbf{x}_{l-1}) = \mathcal{F}_l^{l+k}(\mathbf{x}_{l-1}) + \mathbf{x}_{l-1}$. Such a residual mapping can be achieved by means of identity mapping, namely, by using identity shortcut connections skipping $k+1$ layers.

A diagram of our end-to-end deep residual neural network with dilated convolutions can be seen in Fig. 5. The proposed deep residual learning architecture for MI detection and localization is originally based on research studies for keyword spotting presented in [55] and [56]. However, for this research, the architecture is significantly revised.

In this research, we consider a front-end based on one-dimensional convolutional layers (1-C), which to the best of our knowledge, is novel in the context of MI detection and localization. Our analysis shows that such front-end provides better performance compared to directly feeding the multi-lead ECG signal matrix into the first two-dimensional (2D) convolutional layer of the deep residual neural network as in [38].

We have extensively analyzed the proposed model with different number of filters, kernel sizes, and stride numbers to find the high performance 1D convolutional layers. The parameters of the proposed CNN model are 20 filters, zero bias vectors, a kernel size of 100 samples, and a stride of 50 samples. It is noteworthy that this set-up yields a *pseudo*-time–frequency representation of the ECG signal, where the number of filters of the layers would correspond to the number of frequency bins. Moreover, the kernel size and stride match the length of the analysis window and its hop size, respectively. Therefore, with sampling rate of 100 Hz, it is equivalent to using 20 *pseudo*-frequency bins and a 1-second long analysis window with 50% overlap.

After applying a rectified linear unit (ReLU) activation function, each lead is represented by a 9×20 *pseudo*-time–frequency matrix. Then, the twelve *pseudo*-time–frequency matrices (one from each of the 12 leads) are stacked across the depth dimension and the resulting $9 \times 20 \times 12$ feature volume is fed into the first 2D convolutional layer of our architecture. Following the shallowest 2D convolutional layer, there is a total of three residual blocks with identity mapping. In each residual block, there are two convolutional layers, each followed by a ReLU activation function, and one batch normalization layer for regularization purposes [57]. The six convolutional layers of the residual blocks apply dilated convolutions to increase the receptive field of the network [58]. For each layer, the dilation rate depends on the layer position within the network. Thus, the dilation rates of the convolutional layers in the first and second residual blocks are $(1, 1)$ and $(2, 2)$, respectively. Additionally, the dilation rates of the first and second convolutional layers of the third residual block are, respectively, $(4, 4)$ and $(8, 8)$. A non-residual convolutional layer with $(16, 16)$ convolution dilation, another batch normalization layer, and an average pooling layer are appended to the third residual block. Then, for MI detection and classification, a fully-connected layer with softmax activation is employed. Finally, it is worth mentioning that each of the 2D convolutional layers have 7 filters (equal to the number of neurons in the fully-connected layer), zero bias vectors, and a kernel size of 3×3.

3. Dataset and materials

The national Metrology Institute of Germany, also known as Physikalisch-Technische Bundesanstalt (PTB), provides a free digitized ECG database for the purpose of research and education through PhysioNet bank [42,59]. The PTB database has been widely used in MI detection and localization studies [19,23,24,26,60]. There are 549 records of conventional 12-leads ECG signals known as I, II, III, aVR, aVL, aVF, V1–V6. Each signal is recorded at 1000 Hz sampling rate and 16 bits amplitude resolution over a range of ± 16.384mV.

The records belong to 290 subjects aged from 17 to 85 years old. 72% of subjects are male with mean age of 57.2 and 28% of subjects are female with mean age of 61.6 years old. The clinical summary for 22 subjects were not available in the dataset and excluded from this study. 148 subjects or correspondingly 368 out of 549 records are labeled as MI cases and the number of subjects that are labeled as healthy cases are 52 (80 records).

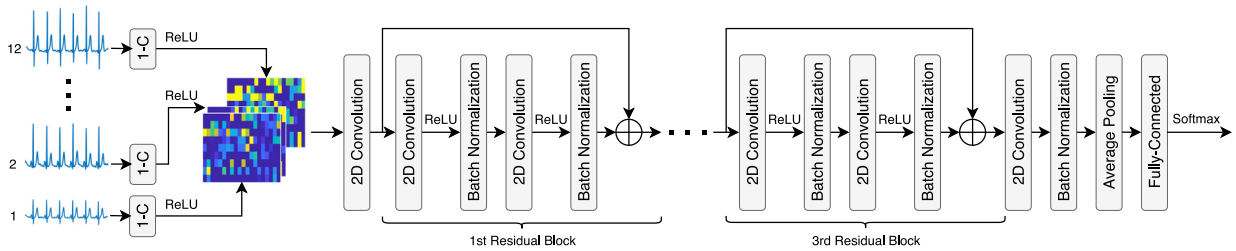

Fig. 5. Diagram of the proposed end-to-end deep residual neural network for MI detection and localization (1-C stands for one-dimensional convolutional layer).

Table 2
The distribution of data between the classes.

MI location	No. of segments	Overlap (%)
Normal	1886	10.0
Anterior (AMI)	1861	50.0
Antero-Lateral (ALMI)	1775	50.0
Antero-Septal (ASMI)	2005	20.0
Inferior (IMI)	2000	10.0
Infero-Lateral (ILMI)	1853	40.0
Infero-Postero-Lateral (IPLMI)	1861	80.0

Table 3
MI detection performance (average, standard deviation, and maximum) with respect to different number of PCs (N_{pc}) using classic hierarchical approach. $N_{pc} = 7$ is selected for feature extraction.

N_{pc}	Accuracy			Sensitivity			Specificity		
	Average	Std.	Max.	Average	Std.	Max.	Average	Std.	Max.
2	90.63	1.31	91.25	90.35	1.73	92.22	90.92	1.94	93.33
3	96.55	0.79	98.25	96.60	1.88	97.56	96.50	1.58	97.89
4	97.30	0.92	99.17	96.85	1.94	97.67	97.75	1.21	98.33
5	98.09	1.15	99.58	97.60	2.45	98.63	98.58	1.27	99.25
6	98.88	0.82	99.58	98.60	2.38	99.17	99.17	0.66	100.00
7	99.11	0.88	99.73	98.83	1.61	99.46	99.39	1.02	100.00
8	97.88	1.03	99.58	97.77	2.85	98.33	98.00	1.63	100.00

Other subjects are labeled with heart diseases unrelated to MI such as branch block and consequently are excluded from this study.

For this study, the data is segmented into 5-second long samples from 12-lead signals, constructing 5968 segments labeled with six different classes. In order to balance the data distribution and keep the prior probabilities equal, resampling with an adjustable overlap percentage is used for signal windowing as shown in Table 2. Note that this data is completely de-identified and publicly available; therefore no ethics statement was acquired for this investigation.

In order to properly train and validate the classification methods, the data is divided into three sets. 60% of the data is allocated as the training dataset, 10% is separated for validation and the rest is considered as the test dataset. As mentioned earlier, unlike many of the previous studies, we employed a patient-independent approach in which samples from a given subject are ensured to be only included in one of the training, validation or testing datasets. Otherwise, although the nominal accuracy of the constructed classification methods might be very high, the model is highly over-fitted and there is no guarantee that the model reaches similar accuracy for an unseen cases. Additionally, in order to suppress the effect of initialization in the constructed networks, a K-fold cross validation method (K=5) is implemented. Feature scaling and normalization are also conducted to standardize the features with a zero mean and unit standard deviation.

4. Results

In this section, results of the classic model and the end-to-end deep residual network on the PTB data-set are analyzed and compared. The classifiers' performance are measured in terms of accuracy (*Acc*), sensitivity (*Sn*), and specificity (*Sp*). The *Acc* of a classifier is the ratio of the correct predictions to the total number of predictions. The *Sn*, also called recall or true positive rate (TPR), measures the proportion of positive predictions that are correctly identified over all positive cases. On the other hand, *Sp*, also called true negative rate (TNR), is an indicator of the proportion of negative predictions that are correctly identified as such. *Acc*, *Sn*, and *Sp* are defined by Eqs. (3), (4) and (5), respectively. In the binary classification settings, *TP*, *TN*, *FN* and *FP* indicate the number of true positives, true negatives, false positives and false negatives, respectively.

$$Acc = \frac{TP + TN}{TP + FN + TN + FP} \tag{3}$$

$$Sn = \frac{TP}{TP + FN} \tag{4}$$

$$Sp = \frac{TN}{TN + FP} \tag{5}$$

These performance metrics can be expanded for classification problems with more than two classes. Let n represent the number of samples in a given data-set and k be the number of classes. Therefore, n_k denotes the sample proportion of kth class, while n'_k indicates the number of samples labeled as the kth class. Using these information and constructing the confusion matrix for a multi-class problem, c_{kg} represents the number of samples belonging to class k but labeled as class g. Consequently, the diagonal elements c_{kk} represent the number of correctly classified samples in class k, and non-diagonal elements denote the numbers of miss-classification samples. According to the above definition, sensitivity and specificity of each class and the overall accuracy of the classifier can be calculated as follows [61]. Note that the overall sensitivity and specificity of the classifier is the average performance of each class.

$$Acc = \frac{\sum_{k=1}^{K} C_{kk}}{n} = \sum_{k=1}^{K} Sn_k \frac{n_k}{n} \tag{6}$$

$$Sn_k = \frac{C_{kk}}{n_k} \tag{7}$$

$$Sp_k = \frac{\sum_{\substack{g=1 \\ g \neq k}}^{K} (n_g - C_{gk})}{n - n_k} \tag{8}$$

4.1. Results pertaining to classic approach

4.1.1. MI detection

In order to build high performance detection system with lowest number of extracted features, the model is trained with different N_{pc} and evaluated on the validation data-set. Using 5-fold cross validation, the accuracy, sensitivity, and specificity of

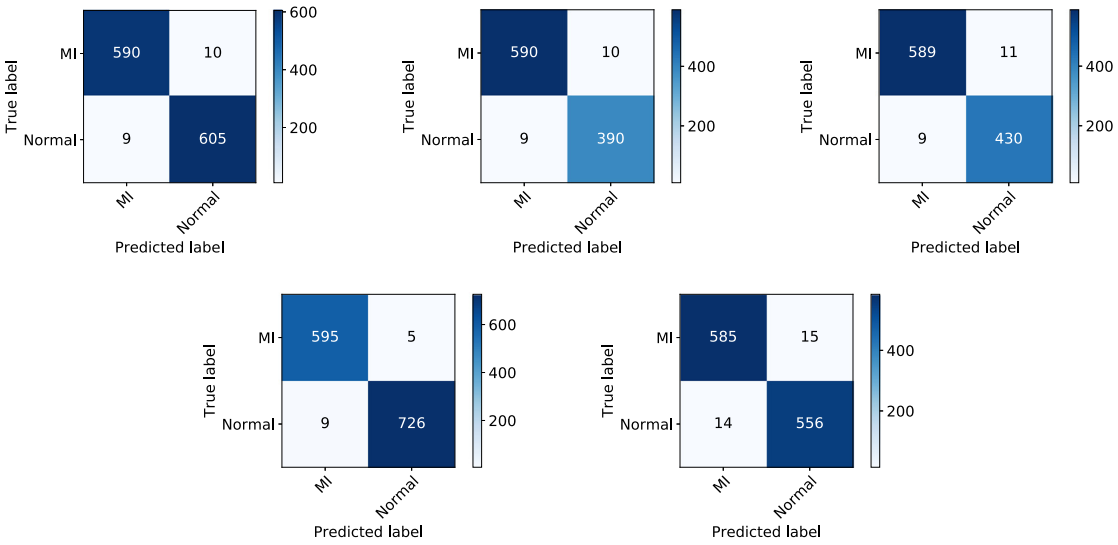

Fig. 6. Confusion matrices of MI detection in classic approach. From left to right and top to bottom: confusion matrices from the 1th, 2th, 3th, 4th, and 5th cross-validation folds.

Table 4
MI detection performance over 5-fold cross-validation ($N_{pc} = 7$).

Performance metric	Fold 1	Fold 2	Fold 3	Fold 4	Fold 5	Average	Std.
Accuracy	98.43	98.10	98.08	98.95	97.52	98.21	0.52
Sensitivity	98.50	98.50	98.49	98.51	97.66	97.50	0.37
Specificity	98.37	97.50	97.51	99.32	97.37	98.01	0.83
Positive predictive value	98.33	98.33	98.17	99.17	97.50	98.30	0.59
Negative predictive value	98.53	97.74	97.95	98.78	97.54	98.11	0.53

classification performance for each N_{pc} is presented in Table 3. As N_{pc} increases, the overall performance of the classifier improves. However, the increase in N_{pc} may introduce unnecessary variation in the model, leading to overfitting. As a result, although the model performance may be higher in training phase, it may decrease once the model is assessed on the validation data-set. More specifically, in the cases of N_{pc} equals to 5, 6, 7, training procedures are executed properly with the average accuracy higher than 98.09% and increasing N_{pc} to 8, have not improved the accuracy of the model. Thus, N_{pc} is selected for the analysis acquiring average accuracy of 99.11%, sensitivity of 98.83%, and specificity of 99.39%. The standard deviation of each constructed signal resulting from PCA is also calculated and used for the feature set. Therefore, based on the given results, 12-lead ECG selected sub-band coefficients are transformed by PCA, and only the first seven PCs have be taken in the feature extraction step.

5-fold patient independent cross-validation test is conducted on features extracted from seven PCs and the results are shown in Table 4 and Fig. 6. Overall accuracy of 98.21%, sensitivity of 97.50% and specificity of 98.01% are obtained for diagnosing the infarcted subjects.

4.1.2. MI localization

The same procedure to compute distinctive features as carried out for MI detection is performed. Using different N_{pc} in feature extraction phase, the performance of the shallow NN classifier is computed on the validation data-set. As shown in Table 5, the MI location accuracy of each region is individually assessed. Accordingly, $N_{pc} = 8$ is selected for MI localization classifier.

Similarly, patient-independent 5-fold cross-validation datasets are constructed and the NN is evaluated. The confusion matrices corresponding to each of the cross-validation datasets are given in Fig. 7. The error in classification of patients in different datasets

Table 5
MI localization performance in classic hierarchical approach with respect to the different N_{pc}.

Performance metric	MI location	Number of principal components						
		2	3	4	5	6	7	8
Sensitivity	ILMI	0.813	0.891	0.935	0.959	0.969	0.974	0.979
	AMI	0.802	0.880	0.932	0.956	0.967	0.976	0.984
	IPLMI	0.822	0.898	0.944	0.965	0.974	0.978	0.986
	ASMI	0.799	0.881	0.933	0.956	0.967	0.972	0.978
	IMI	0.797	0.881	0.932	0.955	0.969	0.978	0.986
	ALMI	0.804	0.881	0.935	0.960	0.969	0.978	0.984
Specificity	ILMI	0.970	0.984	0.990	0.994	0.996	0.996	0.996
	AMI	0.960	0.972	0.984	0.992	0.992	0.992	0.994
	IPLMI	0.965	0.984	0.993	0.997	0.997	0.998	0.998
	ASMI	0.966	0.981	0.990	0.992	0.996	0.996	0.996
	IMI	0.961	0.982	0.989	0.991	0.996	0.996	0.996
	ALMI	0.966	0.981	0.991	0.995	0.994	0.995	0.995
Accuracy	ILMI	0.872	0.933	0.947	0.968	0.975	0.984	0.989
	AMI	0.846	0.921	0.955	0.965	0.977	0.985	0.989
	IPLMI	0.952	0.974	0.991	0.989	0.997	0.995	0.997
	ASMI	0.807	0.888	0.937	0.963	0.961	0.975	0.979
	IMI	0.818	0.882	0.938	0.960	0.972	0.979	0.986
	ALMI	0.833	0.886	0.942	0.968	0.979	0.985	0.989

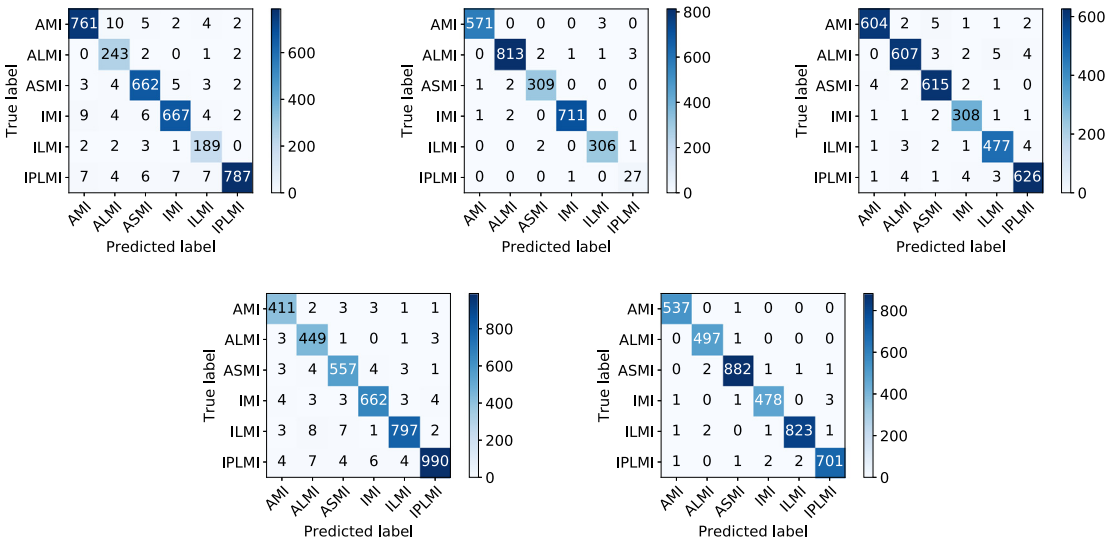

Fig. 7. Confusion matrices of MI localization for classic hierarchical mode. From left to right and top to bottom: confusion matrices from the 1th, 2th, 3th, 4th, and 5th cross-validation folds.

Table 6
MI localization performance of hierarchical classification approach over 5-fold cross-validation ($N_{pc} = 8$).

Performance metric	Fold 1	Fold 2	Fold 3	Fold 4	Fold 5	Average	Std.
Accuracy (%)	96.81	99.27	98.06	97.58	99.42	98.22	1.11
Sensitivity (%)	96.85	98.78	98.05	97.62	99.43	98.14	1.00
Specificity (%)	99.04	99.81	99.46	98.93	99.80	99.40	0.41

Table 7
Performance of deep end-to-end NN for MI detection and localization over 5-fold cross-validation.

Performance metric	Fold 1	Fold 2	Fold 3	Fold 4	Fold 5	Average	Std.
Accuracy (%)	100	99.98	99.98	100	100	99.99	0.01
Sensitivity (%)	100	100	100	100	100	100	0.00
Specificity (%)	100	100	100	100	100	100	0.00

is shown in Table 6. The accuracy of 98.22%, sensitivity of 98.14%, and specificity of 99.40% are obtained.

4.2. End-to-end deep neural network results

Keras [62] was used to implement the end-to-end deep residual learning architecture depicted in Fig. 5. The proportion of model parameters from the twelve one-dimensional convolutional layers is 5,997. This number of parameters is relatively low, compared to the other deep residual learning architectures such as [55] and [56] with more than 200,000 parameters. After random initialization of parameters, deep residual learning models were trained for a total of 20 epochs by considering a multi-class cross-entropy loss function. We used the Adam optimizer [63] with the learning rate and the learning rate decay of 0.001 and 0.00, respectively, $\beta_1 = 0.9$ and $\beta_2 = 0.999$. Moreover, the size of the minibatch, number of samples per gradient update, was set to 32 training examples.

Performance metrics, in percentages, and confusion matrices are shown in Table 7 and Fig. 8, where we have considered 5-fold cross-validation. Our results indicate that the deep end-to-end residual NN are able to achieve *semi*-flawless MI detection and localization over different folds in cross-validation. With miss-classifying only 1 detection case in 2th and 3th folds, the average (i.e., across folds) MI detection and localization accuracy, sensitivity, and specificity is 99.99%, 100%, and 100% respectively.

Compared to the traditional machine learning models, deep learning models are more dependent on the size of training dataset [64,65]. Therefore, we investigate the impact of training size on the accuracy of the model. To that end, 10% of the dataset is reserved for validation and the remaining dataset is divided between training and test datasets. For instance, with 30% training set size, the amount of test dataset is 60%. Fig. 9 illustrates this investigation. The threshold at which the model reaches the minimum acceptable accuracy ($Acc > 99\%$) is 55% of this dataset size. This result indicates that our deep learning model is efficient and does not suffer from overfitting.

5. Evaluation and discussion

In this section, we first investigate the importance of applying PCA transformation on the overall performance of the classic approach. Then, we compare the computational time of the shallow and deep end-to-end NN models. Finally, we summarize the state-of-the-art proposed methods along with their reported performance metrics.

In the classification and pattern recognition literature, there is often a positive correlation between the feature vector size and the obtained accuracy. To verify this conjecture, we trained the model with and without PCA transformation and compared the performance of the shallow hierarchical NN classifiers. In the model without PCA reduction, the entire 48 features are fed into the model which resulted in Accuracy of 90.37%, Sensitivity of 88.71%, and Specificity of 91.88%. However, with PCA reduction, the model achieves higher performance for MI detection ($Acc = 98.21\%$, $Sn = 97.50\%$, and $Sp = 98.01\%$). With the similar results obtained from MI localization comparison, we conclude that while PCA technique reduces the number of ECG signals from 48 to 28 (for detection) and 32 (for localization), the performance of the classification has not degraded but improved.

In the second method (deep end-to-end NN), we use a single 1D convolutional layer per ECG lead to extract a *pseudo*-time–frequency representation. This information is utilized to create a compact and discriminative input feature volume to attain the strengths of a deep residual learning architecture. The superiority in performance of the proposed end-to-end method compared to the classic one is significant. However, due to larger number of hidden layers and parameters in the deep NN, the computational time to train deep NN is remarkably longer. The computational

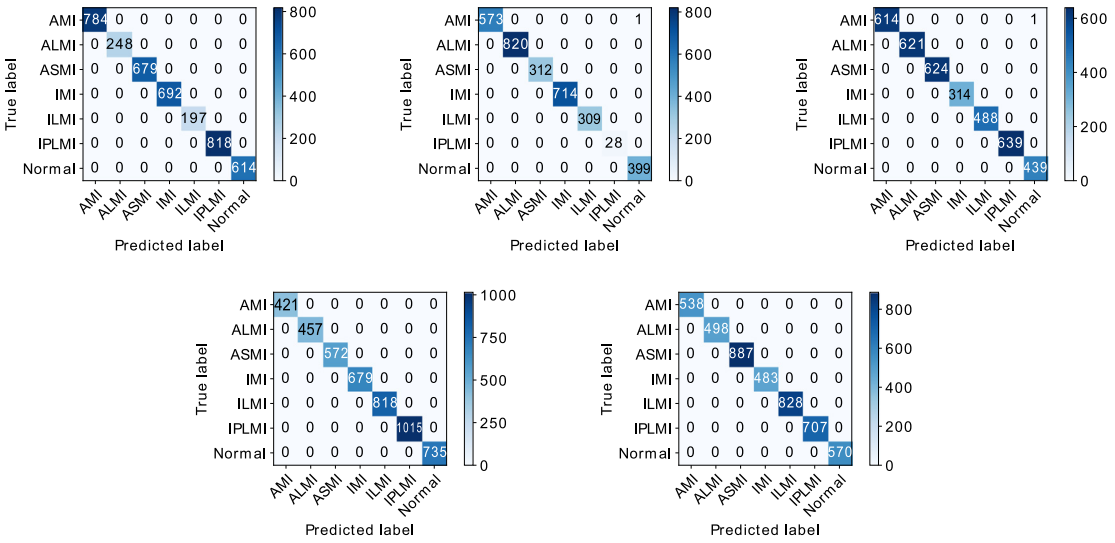

Fig. 8. Confusion matrices for MI detection and localization using deep end-to-end NN. From left to right and top to bottom: confusion matrices from the 1th, 2th, 3th, 4th, and 5th folds.

time of training phase for deep NN was 1475.5 ± 110.37 s, compared to 480.5 ± 53.2 s for classic hierarchical approach. The computational time for pre-processing, frame segmentation and feature extraction for each sample took 0.46 and 0.09 s for classic and end-to-end approaches, respectively. However, once the classifiers are trained, both methods would detect and localize MI patient from the test data set within milliseconds (i.e., 0.01 to 0.02 s). Note that the models are run on a personal computer with Intel Core i5-7500 Quad-core 3.40 GHz and Nvidia GeForce GTX 1070.

In order to signify the performance of our proposed model, a summary of recent MI detection and localization literature is provided in Table 8. This summary collects the reported results of studies where PTB database is used. The table compares these studies based on feature extraction and classification methods, number of leads, the reported features, and performance metrics of MI detection and localization methods. Note that, end-to-end techniques require no feature extraction methods, since the classifier can automatically generate the features. In this table, training set ratio is also reported as a noteworthy information to assess the complexity of classification methods used in each study. Since our two proposed methods are significantly different after pre-processing phase, each method is reported individually.

One of the early studies on automating MI classification was proposed by Arif et al. [24]. Authors employed 36 time-domain features, a pruning algorithm, and kNN for 10 classes of MI and reported 96.72% and 99.97% specificity from their classifiers. Acharya et al. [25] used 125,652 healthy and 485,753 MI beats and built a kNN classifier with 47 features to detect MI and 25 features to localize 10 MI classes, respectively. Le et al. [23] proposed a method based on capturing the complex cardiac excitation and propagation dynamics as a random-walk network reconstructed from VCG signals. For this purpose, they extracted 161 features from VCG signals and their random-walk representation for MI localization. Using statistical tests (i.e., Anderson–Darling and Kolmogorov Smirnov), the number of features were reduced to 10 and fed into a hierarchical classification and regression tree (CART), resulting a sensitivity of ∼ 88% and a specificity of ∼ 92% (with standard deviation < 5%). Dohare et al. [21] used PCA to reduce the number of features from 220 to 14 and classified MI patients using RBF-SVM classifier. The average computational time for signal processing, training and testing the classifier was 24.5, 12.50, and 0.011 s, respectively.

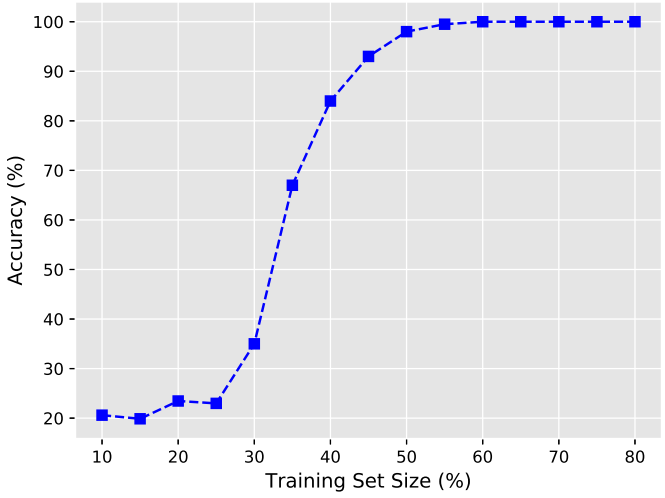

Fig. 9. Training-set size versus classification accuracy for end-to-end deep learning model.

Sharma et al. [26] employed multi-scale energy and the Eigenspace approach for feature extraction. Authors used kNN, linear, and radial basis function (RBF) SVM classifiers among which RBF-SVM achieved the highest accuracy. For MI detection, 60 extracted features resulted in 96% accuracy and for MI localization, 72 extracted features resulted 99.58% accuracy for SVM classifier with 6 classes. Computational time for training the MI detection and localization classifiers were 56.67 and 58.5 s, respectively. The method carried out by Noorian et al. [66] converted the signals to VCG signals and only used the magnitude vector which forfeited the valuable spatial information of the leads, particularly in MI localization. Authors reported 95.35% accuracy from one single run, which was experimented on a subset of 50 out of 368 MI records.

Exploring the MI detection literature that used CNN, Liu et al. [32] used 1D convolutional layers for the definition of feature extraction branches on a lead basis. Authors only distinguished among five different locations of the MI with the accuracy of 94.82%. In our second proposed method, we used up to three 1D convolutional and additional three mean-pooling layers per ECG lead providing a vector to a much simpler classifier consisting

Table 8
Summary of recent studies for automated MI detection and localization where 12-lead ECG signals are obtained from PTB database; **Ftrs**: number of hand-crafted features, ***Sn***: Sensitivity, ***Sp***: Specificity, ***Acc***: Accuracy, n_k: Number of classes, **P.M.**: Proposed Method.

Ref.	Feature extraction method	Classification method	Training set ratio	Number of leads	MI detection				MI localization				
					Ftrs	*Sn*(%)	*Sp*(%)	*Acc*(%)	Ftrs	*Sn*(%)	*Sp*(%)	*Acc*(%)	n_k
[18]	ST segmentation	LTMIL+kNN†, LTMIL+SVM, LTMIL+NN, LTMIL+RF	90%	12	74	92.30	88.10	–					
[24]	Time-domain	Pruning algorithm, kNN†	50%	12	36	99.97	99.90	–	36	96.72	97.11	–	10
[23]	VCG	Classification and regression tree (CART)	–	3	10	–	–	91.00		88	92	89.1	3
[66]	VCG, PCA	RBF-NN	70%	3	9	94.23	99.09	–	9	–	–	95.35	10
[26]	Multi-scale energy DWT	SVM†, kNN	25%	12	60	93.00	99.00	96.00	72	–	–	99.58	6
[60]	Polynomial function fitting	Decision tree†, Random tree, Naive Bayes, SVM	50%	2	88	–	–	94.40					
[25]	DWT	kNN	90%	12	47	99.45	96.27	98.80	25	99.55	99.16	98.74	10
[31]	SWT	CNN†, SVM	99%	3	84	85.33	84.09	84.54					
[21]	PCA	SVM	50%	12	14	96.60	96.60	96.60					
[36]	DFT	Logistic regression†, Threshold based model	80%	3	6	96.50	92.70	95.60					
[34]	‡	13-layer deep neural network	63%	1	0	99.79	97.44	99.34					
[32]	‡	Multi-branch CNN	80%	12	0	98.73	99.35	98.79	0	–	–	94.82	5
[40]	Fourier–Bessel series expansion, EWT	Deep layer least square SVM	70%	12	108	99.87	99.60	99.74					
[38]	‡	Fully connected CNN	90%	8					0	93.3	89.7	–	3
P.M.1	DWT, PCA	NN	60%	12	28	97.5	98.01	98.21	32	98.14	99.40	98.22	6
P.M.2	‡	Deep end-to-end NN	60%	12					0	100	100	100	7

(†) indicates the classifier with the highest performance that is being reported in this table.
(‡) indicates the studies that did not use any feature extraction methods.
(–) indicates the information that was not reported in the original study or could not be computed from the study.

of a fully-connected layer with softmax activation. The relatively high computational complexity of the feature extraction branches in [32] causes large number of parameters. In summary, our second proposed method, deep residual neural network model, is able to achieve near perfect MI detection and localization performance with less computational complexity as well as detecting an additional MI location (i.e., infero-postero-lateral).

Deep residual network also has been previously employed for MI detection and localization by Strodthoff et al. [38]. Apart from healthy subjects, authors only distinguish between two rough classes colloquially designated as anterior myocardial infarction (aMI) and inferior myocardial infarction (iMI). In their approach, the multi-lead ECG signal is arranged into a matrix that serves as input to the first two-dimensional convolutional layer of the deep residual learning architecture. However, in our work, inspired by speech waveform processing with neural networks [67], we found a more robust front-end consisting of the use of 1D convolutional layers to obtain an intermediate two-dimensional representation for each lead of the ECG signal. These intermediate representations are then stacked across the depth dimension and the resulting feature volume is fed into the first two-dimensional convolutional layer of our deep residual neural network, which, also unlike [38], uses dilated convolutions and has a different structure.

6. Conclusion

The timely diagnosis of myocardial Infarction (MI) is very critical to save lives. To automate diagnose and localize MI, two classification methods are developed and evaluated, using 12-lead electrocardiograms. Machine learning and deep learning methods have shown several similarities and differences in their implementation, applications, and associated performance. This research aimed to highlight the differences in the prerequisite steps of classic and deep machine learning methods for processing ECG signals and evaluate their outcomes. In the classic approach, after the ECG signals are preprocessed, the discrete wavelet transform and principal component analysis are employed as the transformations techniques to extract distinctive feature sets from the signals. A two-class Neural Network classifier is developed to diagnose infarcted subjects by employing 28 features. Then, a multi-class NN is constructed to localize the infarcted part of myocardium by employing 32 features. The average accuracy of 98.21% and 98.22% is achieved in detection and localization, respectively. Our proposed MI detector outperforms other reported classifiers that have used the same database.

With the rise of deep learning, several studies report improved results compared to classical machine learning methods for the aforementioned problem. Therefore, we also developed a novel end-to-end deep residual learning model that achieves *semi*-perfect classification for MI detection and perfect MI localization. In this method, only preprocessing step was required prior to applying end-to-end deep learning architecture with dilated convolutions. Consequently, the proposed framework can be confidently examined and utilized by clinical datasets that are largely unstructured and the distribution of classes are highly imbalanced.

While the proposed model shows the benefits of using deep learning technique to detect and localize the MI from ECG signals that are previously recorded, a future challenge is to develop a hardware that proactively detects MI disorders. One recommendation is attaching an extra electronic circuit to the standard ECG monitoring machines in the emergency room so that the ECG

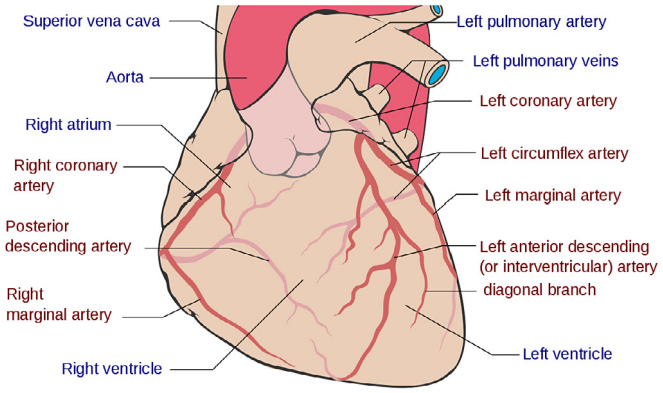

Fig. A.10. Coronary arteries structure. LCA and RCA are the main arteries which supply several branches [68].

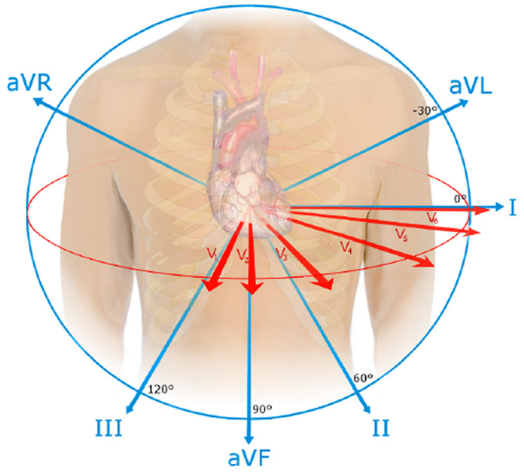

Fig. A.11. ECG 12-lead viewpoints. There are six limb leads permit vertical viewpoints and six chest leads permit horizontal viewpoints to the electrical activity of the heart [69].

Table A.9
ECG leads and corresponding viewpoints to the electrical activity of the heart.

Views of the Heart	Leads
Interior	II, III, aVF
Lateral	I, aVL, V5, V6
Anterior	V3, V4
Septal	V1, V2

machine can simultaneously detect and localize any MI disorders while being used for monitoring and recording patient's ECG signals.

CRediT authorship contribution statement

Kamal Jafarian: Conceptualization, Methodology, Investigation, Writing - original draft. **Vahab Vahdat:** Formal analysis, Project administration, Supervision, Writing - original draft. **Seyedmohammad Salehi:** Investigation, Methodology, Visualization, Writing - review & editing. **Mohammadsadegh Mobin:** Supervision, Validation, Writing - review & editing.

Declaration of competing interest

The authors declare that they have no known competing financial interests or personal relationships that could have appeared to influence the work reported in this paper.

Acknowledgments

Authors want to thank the reviewers and editor-in-chief of Applied Soft Computing, for their insightful comments. We are also grateful to Dr. Ivan Lopez-Espejo, Department of Electronic Systems, Aalborg University, Denmark and Neda Derakhshani, Data Scientist at CVS-Health, for their help with developing end-to-end approach.

Appendix. Coronary anatomy and myocardial infarction

A human heart consists of four major chambers (i.e., right atrium (RA), right ventricle (RV), left atrium (LA), and left ventricle (LV)). The right and left side of the heart have different functions. The right side of the heart receives de-oxygenated blood from the veins and pumps that through the pulmonary artery into the lungs for purification. On the other hand, the left side of the heart receives the oxygenated blood from the lungs and pumps that toward the body organs through the aorta [2]. The heart functionality is highly dependent on the coronary circulation system that supplies oxygenated blood directly toward cardiac muscles to keep the heart nourished and oxygenated. The coronary circulation system is comprised of several small vessels and coronary heart disease can cause myocardial infarction (MI) leading to the insufficient supply of nutrients and the oxygen-rich blood to a section of heart muscle [2].

As illustrated in Fig. A.10, two principal coronary arteries that are derived from the aorta are left coronary artery (LCA) and right coronary artery (RCA). The LCA basically supplies the left side of the myocardium consisting of the left ventricle and the left atrium. Moreover, LCA branches off into the left anterior descending (LAD) which supplies the anterior wall of the left ventricle, and left circumflex (LCX) that equips the lateral wall of the left ventricle [2,4]. In addition, the RCA divides into smaller branches, the posterior descending artery (PDA) and the acute marginal artery (AMA) which supply blood mainly to the right atrium and ventricle walls. The RCA occlusion can cause conduction abnormalities and increase the risk of bradycardia and the atrioventricular block [2,4]. The occlusion of LAD, which is the most commonly occluded artery, can cause right or left bundle branch block, ventricular tachycardia and cardiac dysrhythmias [4].

The electrical impulses generated by the myocardium regulate the beating of the heart or its rhythm. This rhythmical system is vulnerable to cardiovascular diseases, especially in cases that a patient suffers from ischemia of heart muscles [2]. A better understanding of the pathophysiology of the MI has been obtained using 12-lead ECG as a principal method to detect and localize MI. By employing this technique, more efficient and effective treatment plan can be built for the patients suffering from the MI or other acute coronary syndromes [2,4,70].

Electrocardiogram monitors the electrical activity and rhythm of the heart. There are six limb leads called lead I, II, III, aVL, aVR and aVF, which enable vertical viewpoints to the electrical activity of the heart, and six chest or pre-cordial leads, V1 to V6, which allow horizontal viewpoints to the electrical activity of the heart [70]. The arrangement of ECG leads can yield a distinctive anatomical connection which is provided in Table A.9 and Fig. A.11.

References

[1] WHO, Cardiovascular diseases, 2017, http://www.who.int/cardiovascular_diseases/en/.

[2] J. Hall, Guyton and Hall Textbook of Medical Physiology, Elsevier, 2015.

[3] A.T.F. Members, F.V. de Werf, J. Bax, A. Betriu, C. Blomstrom-Lundqvist, F. Crea, V. Falk, G. Filippatos, K. Fox, K. Huber, Management of acute myocardial infarction in patients presenting with persistent ST-segment elevation: The task force on the management of ST-segment elevation acute myocardial infarction of the European Society of Cardiology, Eur. Heart J. 29 (2008) 2909–2945.

[4] A. Kucia, T. Quinn, Acute Cardiac Care: A Practical Guide for Nurses, John Wiley & Sons, 2013.

[5] Y.-C. Yeh, W.-J. Wang, C.W. Chiou, Cardiac arrhythmia diagnosis method using linear discriminant analysis on ECG signals, Measurement 42 (2009) 778–789.

[6] Y.-C. Yeh, W.-J. Wang, C.W. Chiou, A novel fuzzy c-means method for classifying heartbeat cases from ECG signals, Measurement 43 (2010) 1542–1555.

[7] L. Lu, J. Yan, C.W. de Silva, Feature selection for ECG signal processing using improved genetic algorithm and empirical mode decomposition, Measurement 94 (2016) 372–381.

[8] X. Wan, Y. Li, C. Xia, M. Wu, J. Liang, N. Wang, A T-wave alternans assessment method based on least squares curve fitting technique, Measurement 86 (2016) 93–100.

[9] S. Sahoo, B. Kanungo, S. Behera, S. Sabut, Multiresolution wavelet transform based feature extraction and ECG classification to detect cardiac abnormalities, Measurement 108 (2017) 55–66.

[10] C.H. Peels, C.A. Visser, A.J.F. Kupper, F.C. Visser, J.P. Roos, Usefulness of two-dimensional echocardiography for immediate detection of myocardial ischemia in the emergency room, Am. J. Cardiol. 65 (1990) 687–691.

[11] D.-Y. Tsai, K. Kojima, Measurements of texture features of medical images and its application to computer-aided diagnosis in cardiomyopathy, Measurement 37 (2005) 284–292.

[12] R.J.D. Winter, R.W. Koster, A. Sturk, G.T. Sanders, Value of myoglobin, troponin T, and CK-MB mass in ruling out an acute myocardial infarction in the emergency room, Circulation 92 (1995) 3401–3407.

[13] J. McCord, R.M. Nowak, P.A. McCullough, C. Foreback, S. Borzak, G. Tokarski, M.C. Tomlanovich, G. Jacobsen, W.D. Weaver, Ninety-minute exclusion of acute myocardial infarction by use of quantitative point-of-care testing of myoglobin and troponin I, Circulation 104 (2001) 1483–1488.

[14] M. Plebani, M. Zaninotto, Diagnostic strategies using myoglobin measurement in myocardial infarction, Clin. Chim. Acta 272 (1998) 69–77.

[15] P. Kora, ECG based myocardial infarction detection using hybrid firefly algorithm, Comput. Methods Programs Biomed. 152 (2017) 141–148.

[16] M. Hammad, A. Maher, K. Wang, F. Jiang, M. Amrani, Detection of abnormal heart conditions based on characteristics of ECG signals, Measurement 125 (2018) 634–644.

[17] S.L. Kasar, M.S. Joshi, A. Mishra, S. Mahajan, P. Sanjeevikumar, Performance enhancement for detection of myocardial infarction from multilead ECG, Artif. Intell. Evol. Comput. Eng. Syst. (2018) 697–705.

[18] L. Sun, Y. Lu, K. Yang, S. Li, ECG analysis using multiple instance learning for myocardial infarction detection, IEEE Trans. Biomed. Eng. 59 (2012) 3348–3356.

[19] P.-C. Chang, J.-J. Lin, J.-C. Hsieh, J. Weng, Myocardial infarction classification with multi-lead ECG using hidden Markov models and Gaussian mixture models, Appl. Soft Comput. 12 (2012) 3165–3175.

[20] M.A. Waduud, E.N. Clark, A. Payne, C. Berry, M. Sejersten, P. Clemmensen, P.W. Macfarlane, Location of the culprit artery in acute myocardial infarction using the ECG, in: 2011 Computing in Cardiology, IEEE, 2011, pp. 417–420.

[21] A.K. Dohare, V. Kumar, R. Kumar, Detection of myocardial infarction in 12 lead ECG using support vector machine, Appl. Soft Comput. 64 (2018) 138–147.

[22] M. Adam, S.L. Oh, V.K. Sudarshan, J.E. Koh, Y. Hagiwara, J.H. Tan, R.S. Tan, U.R. Acharya, Automated characterization of cardiovascular diseases using relative wavelet nonlinear features extracted from ECG signals, Comput. Methods Programs Biomed. 161 (2018) 133–143.

[23] T.Q. Le, S.T. Bukkapatnam, B.A. Benjamin, B.A. Wilkins, R. Komanduri, Topology and random-walk network representation of cardiac dynamics for localization of myocardial infarction, IEEE Trans. Biomed. Eng. 60 (2013) 2325–2331.

[24] M. Arif, I.A. Malagore, F.A. Afsar, Detection and localization of myocardial infarction using k-nearest neighbor classifier, J. Med. Syst. 36 (2012) 279–289.

[25] U.R. Acharya, H. Fujita, V.K. Sudarshan, S.L. Oh, M. Adam, J.E. Koh, J.H. Tan, D.N. Ghista, R.J. Martis, C.K. Chua, Automated detection and localization of myocardial infarction using electrocardiogram: A comparative study of different leads, Knowl.-Based Syst. 99 (2016) 146–156.

[26] L. Sharma, R. Tripathy, S. Dandapat, Multiscale energy and eigenspace approach to detection and localization of myocardial infarction, IEEE Trans. Biomed. Eng. 62 (2015) 1827–1837.

[27] K. Nezamabadi, Z. Naseri, H.A. Moghaddam, M. Modarresi, N. Pak, M. Mahdizade, Lung HRCT pattern classification for cystic fibrosis using convolutional neural network, Signal Image Video Process. 13 (6) (2019) 1225–1232, http://dx.doi.org/10.1007/s11760-019-01447-y, URL https://doi.org/10.1007/s11760-019-01447-y.

[28] J. Wu, Y. Bao, S.-C. Chan, H. Wu, L. Zhang, X.-G. Wei, Myocardial infarction detection and classification – A new multi-scale deep feature learning approach, in: 2016 IEEE International Conference on Digital Signal Processing, DSP, IEEE, 2016, pp. 309–313.

[29] U.R. Acharya, H. Fujita, S.L. Oh, Y. Hagiwara, J.H. Tan, M. Adam, Application of deep convolutional neural network for automated detection of myocardial infarction using ECG signals, Inform. Sci. 415 (2017) 190–198.

[30] M. Kumar, R. Pachori, U. Acharya, Automated diagnosis of myocardial infarction ECG signals using sample entropy in flexible analytic wavelet transform framework, Entropy 19 (9) (2017) 488.

[31] T. Reasat, C. Shahnaz, Detection of inferior myocardial infarction using shallow convolutional neural networks, in: 2017 IEEE Region 10 Humanitarian Technology Conference, R10-HTC, IEEE, 2017, pp. 718–721.

[32] W. Liu, Q. Huang, S. Chang, H. Wang, J. He, Multiple-feature-branch convolutional neural network for myocardial infarction diagnosis using electrocardiogram, Biomed. Signal Process. Control 45 (2018) 22–32.

[33] H.W. Lui, K.L. Chow, Multiclass classification of myocardial infarction with convolutional and recurrent neural networks for portable ECG devices, Inform. Med. Unlocked 13 (2018) 26–33.

[34] N. Liu, L. Wang, Q. Chang, Y. Xing, X. Zhou, A simple and effective method for detecting myocardial infarction based on deep convolutional neural network, J. Med. Imaging Health Inform. 8 (7) (2018) 1508–1512.

[35] D. Rajan, D. Beymer, G. Narayan, Generalization studies of neural network models for Cardiac disease detection using limited channel ECG, in: 2018 Computing in Cardiology Conference, Vol. 45, CinC, IEEE, 2018, pp. 1–4.

[36] D. Sadhukhan, S. Pal, M. Mitra, Automated identification of myocardial infarction using harmonic phase distribution pattern of ECG data, IEEE Trans. Instrum. Meas. 67 (10) (2018) 2303–2313.

[37] L.D. Sharma, R.K. Sunkaria, Inferior myocardial infarction detection using stationary wavelet transform and machine learning approach, Signal Image Video Process. 12 (2) (2018) 199–206.

[38] N. Strodthoff, C. Strodthoff, Detecting and interpreting myocardial infarction using fully convolutional neural networks, Physiol. Meas. 40 (1) (2019) 015001, http://dx.doi.org/10.1088/1361-6579/aaf34d.

[39] U.B. Baloglu, M. Talo, O. Yildirim, R. San Tan, U.R. Acharya, Classification of myocardial infarction with multi-lead ECG signals and deep CNN, Pattern Recognit. Lett. 122 (2019) 23–30.

[40] R.K. Tripathy, A. Bhattacharyya, R.B. Pachori, A novel approach for detection of myocardial infarction from ECG signals of multiple electrodes, IEEE Sens. J. 19 (12) (2019) 4509–4517.

[41] J. Zhang, F. Lin, P. Xiong, H. Du, H. Zhang, M. Liu, Z. Hou, X. Liub, Automated detection and localization of myocardial infarction with staked sparse autoencoder and treebagger, IEEE Access 7 (2019) 70634–70642.

[42] A.L. Goldberger, L.A. Amaral, L. Glass, J.M. Hausdorff, P.C. Ivanov, R.G. Mark, J.E. Mietus, G.B. Moody, C.-K. Peng, H.E. Stanley, Physiobank, Physiotoolkit, and Physionet, Circulation 101 (2000) 215–220.

[43] M. Blanco-Velasco, B. Weng, K.E. Barner, ECG signal denoising and baseline wander correction based on the empirical mode decomposition, Comput. Biol. Med. 38 (2008) 1–13.

[44] X. Hu, Z. Xiao, N. Zhang, Removal of baseline wander from ECG signal based on a statistical weighted moving average filter, J. Zhejiang Univ. Sci. C 12 (2011) 397–403.

[45] K. Daqrouq, ECG baseline wandering reduction using discrete wavelet transform, Asian J. Inf. Technol. 4 (2005) 989–995.

[46] A. Fasano, V. Villani, Ecg baseline wander removal with recovery of the isoelectric level, in: 2015 Computing in Cardiology Conference, CinC, IEEE, 2015, pp. 577–580.

[47] S.G. Mallat, A theory for multiresolution signal decomposition: The wavelet representation, IEEE Trans. Pattern Anal. Mach. Intell. 11 (1989) 674–693.

[48] L. Sharma, S. Dandapat, A. Mahanta, ECG signal denoising using higher order statistics in wavelet subbands, Biomed. Signal Process. Control 5 (2010) 214–222.

[49] J. Shlens, A tutorial on principal component analysis, 2014, arXiv: 1404.1100.
[50] F. Castells, P. Laguna, L. Sörnmo, A. Bollmann, J.M. Roig, Principal component analysis in ECG signal processing, EURASIP J. Adv. Signal Process. 2007 (1) (2007) 074580.
[51] S. Xu, L. Chen, A novel approach for determining the optimal number of hidden layer neurons for FNN's and its application in data mining, in: International Conference on Information Technology and Applications: ICITA, 2008, pp. 683–686.
[52] D.W. Marquardt, An algorithm for least-squares estimation of nonlinear parameters, J. Soc. Ind. Appl. Math. 11 (1963) 431–441.
[53] M.T. Hagan, M.B. Menhaj, Training feedforward networks with the Marquardt algorithm, IEEE Trans. Neural Netw. 5 (1994) 989–993.
[54] K. He, X. Zhang, S. Ren, J. Sun, Deep residual learning for image recognition, in: Proceedings of CVPR 2016 – Conference on Computer Vision and Pattern Recognition, CVPR, June 26–July 1, Las Vegas, USA, 2016, pp. 770–778.
[55] R. Tang, J. Lin, Deep residual learning for small-footprint keyword spotting, in: Proceedings of ICASSP 2018 – 43rd IEEE International Conference on Acoustics, Speech and Signal Processing, ICASSP, April 15–20, Calgary, Canada, 2018, pp. 5484–5488.
[56] I. López-Espejo, Z.-H. Tan, J. Jensen, Keyword spotting for hearing assistive devices robust to external speakers, in: Proceedings of INTERSPEECH 2019 – 20th Annual Conference of the International Speech Communication Association, September 15–19, Graz, Austria, INTERSPEECH, ISCA, 2019, pp. 3223–3227.
[57] P. Luo, X. Wang, W. Shao, Z. Peng, Towards Understanding Regularization in Batch Normalization, in: International Conference on Learning Representations, 2019.
[58] F. Yu, V. Koltun, Multi-scale context aggregation by dilated convolutions, 2015, arXiv preprint arXiv:1511.07122.
[59] R. Bousseljot, D. Kreiseler, A. Schnabel, Nutzung der EKG-signaldatenbank CARDIODAT der PTB über das internet, Biomed. Tech./Biomed. Eng. 40 (s1) (1995) 317–318.
[60] B. Liu, J. Liu, G. Wang, K. Huang, F. Li, Y. Zheng, Y. Luo, F. Zhou, A novel electrocardiogram parameterization algorithm and its application in myocardial infarction detection, Comput. Biol. Med. 61 (2015) 178–184.
[61] D. Ballabio, F. Grisoni, R. Todeschini, Multivariate comparison of classification performance measures, Chemometr. Intell. Lab. Syst. 174 (2018) 33–44.
[62] F. Chollet, et al., Keras, 2015, https://keras.io.
[63] D.P. Kingma, J. Ba, Adam: A method for stochastic optimization, 2014, arXiv preprint arXiv:1412.6980.
[64] J. Brownlee, Better Deep Learning: Train Faster, Reduce Overfitting, and Make Better Predictions, Machine Learning Mastery, 2018.
[65] J. Cho, K. Lee, E. Shin, G. Choy, S. Do, How much data is needed to train a medical image deep learning system to achieve necessary high accuracy? 2015, arXiv:1511.06348.
[66] A. Noorian, N.J. Dabanloo, S. Parvaneh, Wavelet based method for localization of myocardial infarction using the electrocardiogram, in: Computing in Cardiology 2014, IEEE, 2014, pp. 645–648.
[67] T.N. Sainath, R.J. Weiss, A. Senior, K.W. Wilson, O. Vinyals, Learning the speech front-end with raw waveform CLDNNs, in: Sixteenth Annual Conference of the International Speech Communication Association, 2015.
[68] P.J. Lynch, Coronary Circulation, with Coronary Arteries Labeled in Red Text and Other Landmarks in Blue Text, Wikimedia Commons, 2010, the free media repository, URL https://commons.wikimedia.org/wiki/File:Coronary_arteries.svg.
[69] N. Patchett, Spatial Orientation of EKG Leads, Wikimedia Commons, 2015, URL https://commons.wikimedia.org/wiki/File:EKG_leads.png.
[70] L. Biel, O. Pettersson, L. Philipson, P. Wide, ECG analysis: A new approach in human identification, IEEE Trans. Instrum. Meas. 50 (2001) 808–812.